ACS OMEGA

http://pubs.acs.org/journal/acsodf

Article

Preparation, Characterization, and Evaluation of Curcumin−Graphene Oxide Complex-Loaded Liposomes against *Staphylococcus aureus* in Topical Disease

Mahfoozur Rahman,* Joina Gunjan Singh, Obaid Afzal, Abdulmalik Saleh Alfawaz Altamimi, Majed Alrobaian, Jamshed Haneef, Md. Abul Barkat, Waleed H Almalki, Mayank Handa, Rahul Shukla, Shehla Nasar Mir Najib Ullah, Vikas Kumar, and Sarwar Beg

Cite This: *ACS Omega* 2022, 7, 43499−43509

Read Online

ACCESS | Metrics & More | Article Recommendations | Supporting Information

ABSTRACT: This study describes the development and characterization of curcumin with graphene oxide complex (CUR + GO) loaded into liposomes for treating skin disease. The developed complex was characterized by X-ray diffraction and showed a broad halo pattern, confirming the amorphous nature of the resulting complex. Furthermore, scanning electron microscopy revealed the irregular porous morphology of the complex-highlighting loss of the crystallinity and the emergence of the amorphous phase. Additionally, the liposomes showed long-term stability at 2−8 °C and 25 ± 2 °C/60 ± 5%RH with nonsignificant variations in the particle size, polydispersity index, and zeta potential. Overall, optical and high-resolution transmission electron microscopy images of liposomes showed a consistent shape, and no aggregation with uniform particle size distribution was observed. Furthermore, the cumulative drug release in the first 6 h was 71.24 and 64.24% for CUR-loaded liposomes and CUR-GO-loaded liposomes, respectively. The lower value of drug release might be attributed to the complex development. The drug release model found the first order with non-Fickian diffusion process, which is often observed at higher $n > 0.5$. The antibacterial activity of the CUR with GO-loaded liposome (D2) offered higher anti-microbial activity over other formulations against the mentioned bacterial microorganism that causes skin diseases.

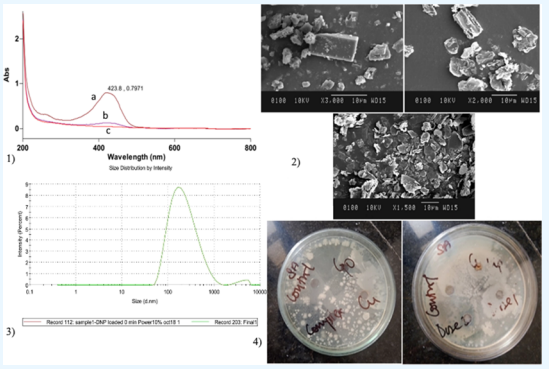

1. INTRODUCTION

Skin infection is more evident nowadays; the infections could be bacterial or fungal.[1] These include psoriasis, eczema, sunburn, leprosy, cellulitis, lupus, and many more. Some common bacteria such as *Staphylococcus aureus*, *Bacillus subtilis*, *Escherichia coli*, and so forth cause severe skin infections and are very common.[1,2] The common infections that they cause on skin and soft tissue are impetigo, folliculitis, furuncles, cellulitis, scalded skin syndrome, and many more.[2−4] There are many treatments and drugs present in the current scenario to deal with these diseases, but they have several issues like adverse effects and limited therapeutic benefits, which requires improvements and changes for the betterment of patients.[5−8] An alternative is the use of phytoconstituents, which is widely employed in topical disease and has gained wider attention.[9,10] Curcumin (CUR) is a lipophilic polyphenol, a yellow−orange natural pigment found in the roots of *Curcuma longa*, which is the primary source.[9,10] There are various studies reported about its antibacterial action against Gram-positive cocci *Staphylococcus aureus* and Gram-negative bacteria entitled *Escherichia coli* and so forth.[10,11] Its therapeutic action has been restricted because of poor solubility, low topical permeability, and inappropriate pharmacokinetic profile.[10,11] Currently, a large number of nanocarriers are being used for the delivery of numerous therapeutic molecules including phytoactives; among these nanocarriers, graphene oxide (GO) has become a potential candidate for drug delivery.[11] GO is an amphiphilic, high-surface-area substance that has considerable potential as a functional carrier for drug delivery.[7,12] Additionally, GO is used for the antimicrobial action because of various physicochemical properties that influence the form of physical interactions with bacterial cells, such as solubility, dispersion, morphology, and size.[13] Furthermore, it exhibited strong cytotoxicity to bacteria and antibacterial activity. According to the reported literature regarding GO dispersion,

Received: June 23, 2022
Accepted: October 17, 2022
Published: November 20, 2022

GO with silver ions showed the highest antimicrobial activity.[8,14] Apart from this, GO and its nanocomposites are reported as drug carriers because they possess lower cytotoxicity and biocompatibility and are extensively studied in drug delivery applications.[13−15] The greatest advantages of the antimicrobial properties of CUR is due to its easy incorporation with GO.[13−15] CUR itself has limited solubility, poor topical sustainability, and limited antimicrobial potential.[16] For this reason, curcumin was conjugated with GO and loaded into liposomes, which may improve the preformulation characteristics.[17,18] By combining both of them, they may show a synergistic response as antimicrobial. Liposomes have received a lot of interest in the topical drug delivery system because of their amphiphilic character, which makes them a superior penetration enhancer for the cutaneous route of administration than traditional formulations.[18−22] Therefore, the objectives of this work were to achieve better antimicrobial actions over the CUR-loaded liposomes. As a result, the primary goal of this work was complex (CUR + GO complex) development, and its characterization was investigated. Finally, the complex was characterized by X-ray diffraction and scanning electron microscopy. Furthermore, the CUR with GO complex-loaded liposomes was developed and characterized. The liposome formulation stability was also tested over a period of three months under various storage circumstances. Finally, the developed liposomal formulation gel formulations were subjected to an in vitro release study, which was compared with CUR-loaded liposomes, and the antimicrobial activity for the complex-loaded liposomes vs CUR-loaded liposomes was investigated.

2. MATERIALS AND METHODS

2.1. Materials. Curcumin was received as a gift sample from Dabur India Limited, Ghaziabad, India. GO was purchased from Sigma-Aldrich Pvt, Ltd. Tripalmitin was purchased from scientific traders, Shastri Marg, Prayagraj. Dimethyl sulfoxide (DMSO) was purchased from BASF SE Ludwigshafen, Germany. Cholesterol was obtained from Loba Chemie Pvt. Ltd., Mumbai, Maharashtra. Dihydrogen sodium hydrogen phosphate was purchased from Loba Chemie Pvt. Ltd., Mumbai, Maharashtra. Potassium dihydrogen phosphate was obtained from Thomas Baker (Chemicals) Pvt. Ltd, Marine Drive, Mumbai, Maharashtra. M/s Bengal Chemicals Ltd. provided absolute ethanol (Kolkata, India). All other substances used in this study were of analytical purity, and double distilled water was employed.

2.2. Methods. *2.2.1. Determination of λ_{max} of Curcumin in DMSO.* CUR was scanned using the ultraviolet−visible (UV−vis) spectrum range of wavelengths 200 to 800 nm (Thermo electron corporation model NO Gensys 10.s). Each sample was diluted with 1.5 mL of DMSO before being maintained in a quartz cell. The double-beam UV−vis spectrophotometer sample was used for the UV scan of CUR, which covered wavelengths from 200 to 800 nm. The spectrometer was calibrated for around 20 min before the cuvette was filled with samples and positioned in the right orientation.[22] A cover was used to keep out any light or scattering so that the absorbance could be maximized. The equipment was allowed to scan through various wavelengths, and the absorbance spectrum was obtained by comparing it to the blank sample and its absorbance graph.[22]

2.2.2. Solubility Studies. Solubility of CUR was quantified by using various lipids, solvents, and solvents. The drug's solubility was tested by diluting a small amount of the drug in several test tubes and adding various solvents. Organic solvents such as methanol, ethanol, acetone, and DMSO are used to dissolve CUR. The solubility of GO organic solvents was also observed in various abovementioned solvents. CUR/GO was also put into each aforesaid vehicle and swirled constantly at 25 ± 1 °C for 72 h to remove any surplus. In addition, furthermore, the supernatant was filtered through a membrane filter with a pore size of 0.45 m after centrifugation at 2000 rpm for 15 min.[18] It was then used to dilute an additional portion of the filtrate, which was then examined by UV spectroscopy at 423 nm. Additionally, the solubility of curcumin was further improved by integrating an excessive quantity of curcumin into the different solvents by shaking in a water bath shaker for 72 h at 37 ± 1 °C. Furthermore, the equilibrated samples were kept under centrifugation at 5000 rpm for 10 min to remove the undissolved medication and filtered using a 0.45 μm filter membrane and assessed using a UV spectrophotometer at λ_{max} of 423 nm.

2.2.3. Development of the Curcumin−GO Complex. The ratio of CUR to GO was taken (1:1). DMSO was used to dissolve both of them. Both were kept on a rotameter for 24 h with regular stirring and a temperature range from 24 to 300 °C. The fluid was then centrifuged for 20 to 30 min at 4000 rpm.[8] Finally, the desiccator was used to remove all of the moisture from the sample.

2.2.4. Characterization of Complex (CUR with GO). 2.2.4.1. X-ray Diffraction. Various films were collected using X-ray diffraction (XRD, PANalytical, Almelo, The Netherlands) techniques and employing 40 mA and 45 kV for the current and acceleration voltage, respectively.[23] An exact 15−20 mg of each sample was placed in a polymethyl methacrylate (PMMA) tube of 25 mm in length. Samples were scanned in a two-dimensional (2D) reflection mode, with a step size of 0.026°, from 5 to 35°. To collect and analyze diffractograms, the X'Pert Data Collector program (version 2.2i) was used.

2.2.4.2. Scanning Electron Microscopy. Scanning electron microscopy (SEM) was used to examine the sample surfaces. A tape of double-sided carbon was used to attach aluminum stubs to each other. A small amount of powder was applied to the tape. In the vacuum chamber of a scanning electron microscope, aluminum stubs were inserted (XL 30 ESEM with EDAX, Philips, Netherlands).[24] A gaseous secondary electron detector (0.8 Torr working pressure, 30.00 kV acceleration voltage) XL 30, Philips, was used for the morphological assessment of the samples (Eindhoven, The Netherlands). The surface properties of the particles were examined under bright light.[24]

2.2.5. Preparation of CUR with GO Complex-Loaded Liposomes. CUR with GO complex (10 mg) was carefully weighed and placed into a 250 mL container of a round bottom flask (RBF). Then, 10 mL of dichloromethane was added to the RBF, which contained cholesterol and tripalmitin in a 2:3 ratio. RBF was held at a decreased pressure and temperature of 200 Pascal and 40 °C ± 2 °C using a rotatory evaporator to obtain a thin dry layer on the inner surface of the RBF by evaporating the solvent. It was kept in a desiccator overnight to ensure that all the organic solvent was removed from the thin dry film.[18] The lipid films were fully hydrated by adding 10 mL of phosphate buffered saline (PBS), shaking briskly for 2−3 min, and then refrigerating overnight. The liposomes were sonicated for 5 min and then again for 5 min to obtain the optimal size.

https://doi.org/10.1021/acsomega.2c03940
ACS Omega 2022, 7, 43499−43509

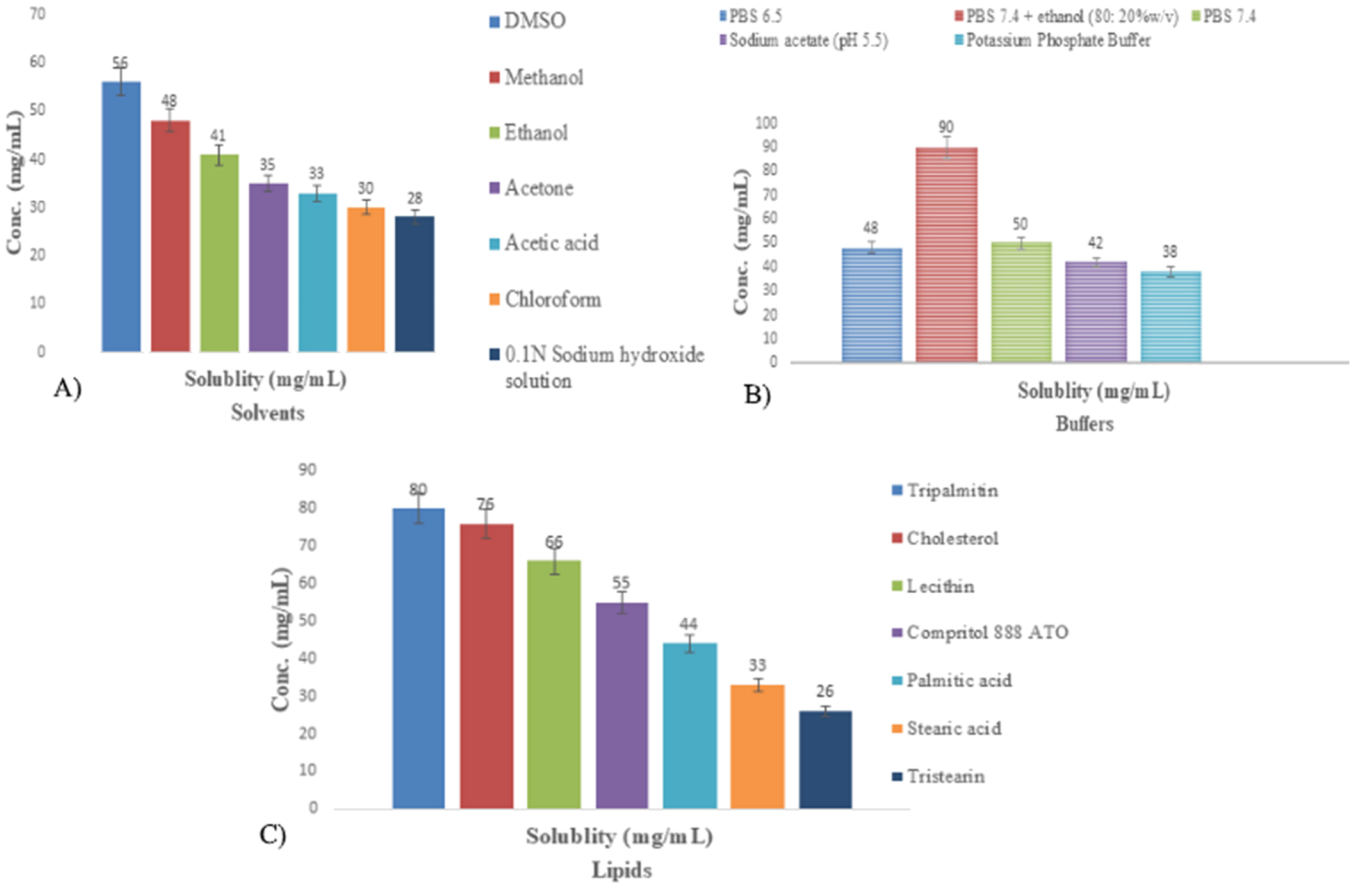

Figure 1. Bar chart depicting the solubility of curcumin in various (A) solvents, (B) buffers, and (C) lipids.

2.2.6. Stability of Liposomes. The formulations were maintained at room temperature for 90 days to ensure their stability. Temperatures of 25 °C ± 2 °C/60% and 40 °C ± 2 °C/75% RH were used to conduct stability tests. The formulation was packaged in 100 g glass jars and hermetically sealed. After 0, 1, 2, and 3 months of storage, the stability was assessed.[25] At each pull, the formulation was checked and did not return to the stability chamber. The particle size (PS), polydispersity index (PDI), and zeta potential of the formulations were measured to determine their ability to maintain colloidal system stability.

2.2.7. Characterizations of Liposomes. The size, PDI, zeta potential, and morphology of the liposomes were evaluated. The liposome size and PDI were estimated by the use dynamic light scattering.[26] A zeta sizer was used to measure electrophoretic mobility under an electric field to determine the zeta potential (Nano ZS, Malvern, U.K.). The morphological surface of liposomes may be studied using this optical microscope (Medilux, Kyowa opticals Co. Ltd., Hashimoto, Japan).[26] The liposomes were evaluated by HR-TEM. Using a diluted solution of liposomes, a drop was deposited on a membrane coated with grids and stained with a drop of 1% phosphor tungstic acid, and the slide was examined.[26] Excess water was drained and the grid was air-dried for 1 min.

2.2.8. In Vitro Drug Releases. For *the* in vitro drug release study, phosphate buffer saline (pH = 7.4) and ethanol (80%: 20%) were used to mimic physiological pH. The liposomes containing CUR and the GO complex were distributed in 2 mL of the appropriate buffer and placed into the dialysis bag. After that, it was placed in 20 mL of release medium. Regular sampling and replacement of medium with fresh samples were used to maintain stable sink conditions.[2] The UV method was used to examine the samples, and the drug release was monitored. Kinetic models for in vitro drug release data were fit using zero-order, first-order Higuchi, Hixon−Crowell, and Korsemeyer models. These data were put through regression analysis.[27] According to these equations, the graphs of the relevant models were drawn. There is a formula for each drug release model listed below.[27] Using fundamental diffusion law correlations, Higuchi sought to establish a link between the drug release rate and the underlying physical constants.

2.2.8.1. Zero-Order-Release Kinetics.

$$Q = Q_0 + k_0 t \quad (1)$$

Q, Quantity of the drug; Q_0, Initial concentration of the drug present in solution; k_0 = zero-order-release constant.

2.2.8.2. First-Order-Release Kinetics.

$$\text{Log } C = \text{Log } C_0 - k_t/2.303 \quad (2)$$

C_0 is the initial drug concentration; C is the concentration after time (t); k is the first-order constant.

The graph shows the relationship between the cumulative log-release percentage and time.

2.2.8.3. Hixson−Crowell-Release Kinetics.

$$Q_0 1/3 - Q_t 1/3 = k_H C_t \quad (3)$$

Q_t is the quantity of drug release at time t; Q_0 represents the initial amount of the drug; $k_H C$ is the rate constant for the Hixson−Crowell rate equation.

https://doi.org/10.1021/acsomega.2c03940
ACS Omega 2022, 7, 43499−43509

2.2.8.4. Higuchi-Release Kinetics. As the square root of a time-dependent process, Higuchi was the first to establish an equation to characterize drug release from an insoluble matrix.

$$Q_t = k_H(t)^{0.5} \quad (4)$$

Q_t is the quantity of the drug released in time t; k_H is the rate constant.

2.2.8.5. Korsemeyer–Peppas-Release Kinetics.

$$M_t/M_o = kt_n \quad (5)$$

M_t/M_o is a fraction of the drug that was released at time t; k is a rate constant; n is the release exponent.

2.3. Antimicrobial Evaluation. *2.3.1. Microorganisms.* The different strains used for the antimicrobial activity were provided by the Department of Industrial Microbiology, Jacob Institute of Biotechnology and Bioengineering, SHUATS. The strains which were used for the study were *Staphylococcus aureus0045.*

2.3.2. Growth Medium. The culture media which is used for the growth of microorganisms *Staphylococcus aureus* was Nutritive Agar (NA). Nutritional agar was used in the ratio of one liter (1 L) for every 31 g of the dehydrated medium.

2.3.3. Agar Well Diffusion Test. The agar well diffusion test is the most commonly used method for testing the antibacterial activity of antimicrobial preparations.[28] In this experiment, a thick layer of NA was put on top of sterile Petri plates in a laminar flow. Spreading 100 μL of the microbial solution over the solidified NA in the Petri plate is the next step in the inoculation process. Wholes were made at a proper distance from each other, and then, the different samples were poured into the wholes ensuring that samples should not come out of the wholes.[28] In the same way, repetitions were made for the microorganism with a control drug in each Petri plate.

3. RESULTS

3.1. Solubility Studies. Figures 1 and 2 show the solubility studies of curcumin in various solvents used in the development of the complex and its formulation. The solubility analysis revealed that the drug was most soluble in the following solvents and buffers. The highest solubility of the drug was found in the DMSO solvent in 56 ± 1.21 mg/mL (shown in Figure 1A) and buffer entitled PBS with ethanol (80:20 v/v) have 90 ± 0.78 mg/mL (Figure 1B). The solubility of the drug in various lipids for developing liposomes is listed in Figure 1C. The highest solubility of the drug in lipid was found in tripalmitin at 80 ± 0.21 mg/mL. The determined solubility of the GO in various solvents is listed in Figure 2A. The highest solubility of GO in the solvent DMSO is 77 ± 0.41 mg/mL. According to the solubility study, we found the solubility of the drugs in various lipids. The solubility of GO in various lipids for developing liposomes is listed in Figure 2B. The highest solubility of GO in lipids was found in tripalmitin at 95 ± 0.22 mg/mL. From the above finding, it is concluded that the highest drug solubility of CUR and GO was observed in solvent DMSO and lipid in tripalmitin. Both selected excipients are to play an important role in the development of liposomes. The higher solubility of the drug in lipids and solvents is an important consideration in topical permeation and drug deposition into the skin.[2]

3.2. Development of Curcumin with the GO Complex. As the method described in Section 2.2.3, at the ratio of 1:1, a thick layer was formed (as shown in Figure S1),

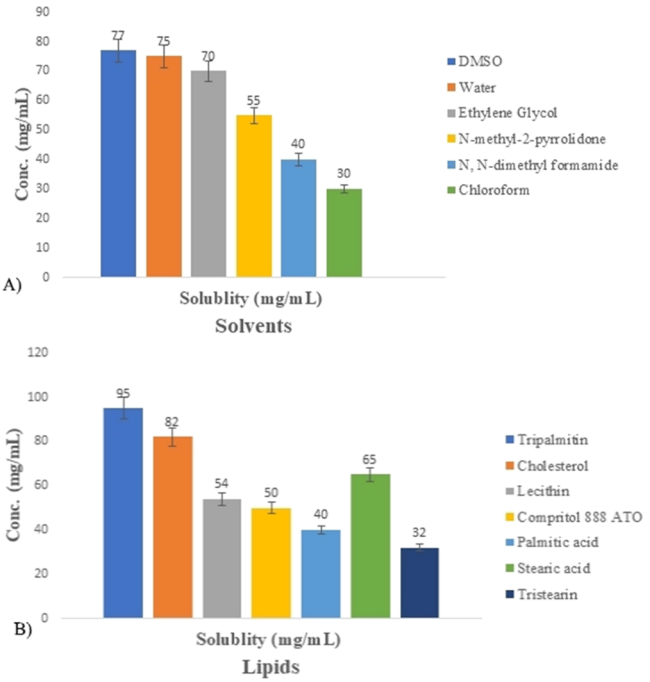

Figure 2. Bar chart depicting the solubility of GO in various (A) solvents and (B) lipids.

and the complex was kept in the desiccator to remove residue moisture. Moreover, the development of the complex is confirmed, as shown in Figure S1. It revealed that the maximum absorbance peak showed the CUR in the UV absorption spectrum at 423 nm (Figure 3a). As a result, the

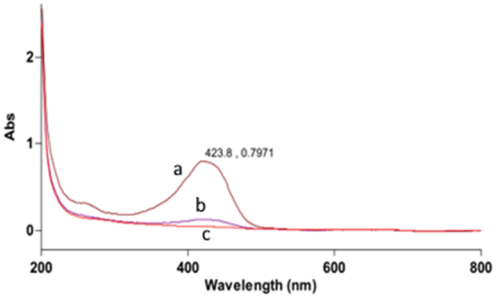

Figure 3. UV absorption spectra of (a) curcumin in DMSO, (b) complex (CUR + GO), and (c) DMSO.

strong peak at this wavelength verified the identification of CUR, which may be attributed to the CUR low energy $\pi-\pi$ excitation.[29] The middle peak shows shifting in the peak, and it confirmed the presence of complex formation (Figure 3b). The base peak represented the peak of DMSO (Figure 3c). Therefore, the above UV spectra data identified CUR and validated the complex formation development.

3.3. Characterization of the Complexes. *3.3.1. X-ray Diffraction.* Figure 4A–D shows the XRD patterns of the lipid (tripalmitin), curcumin (CUR), GO, and complex (CUR + GO). PXRD data DMR indicate a highly crystalline material because of its distinct diffraction pattern. The signature diffraction peaks were observed at different 2θ values viz., 6.5, 13.18, 19.3, 19.5, 22.09, 25.2, and 26.12. Besides, the diffraction peak with the highest intensity was observed at 24.17°, which can be used as a diagnostic peak for its

https://doi.org/10.1021/acsomega.2c03940
ACS Omega 2022, 7, 43499–43509

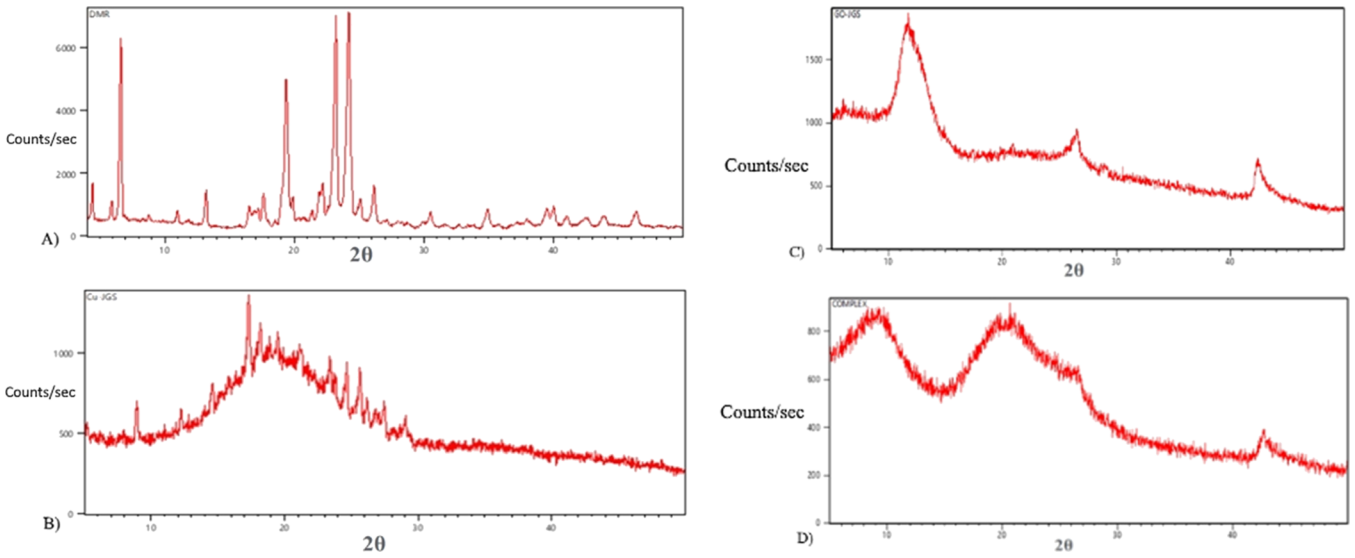

Figure 4. XRD profiles of (A) tripalmitin, (B) CUR, (C) GO, and (D) CUR with the GO complex.

identification. The PXRD pattern of CUR showed that it has a halo pattern with few diffraction peaks, thus indicating partial amorphous nature of sample (Figure 4B) while GO showed an amorphous pattern with broad 2θ peak at 11.2 (Figure 4C). Besides, the PXRD of the complex (CUR with GO) showed a broad halo pattern, confirming the amorphous nature of the resulting complex (Figure 4D). The results showed that the presence of GO facilitates the amorphization of the resulting complex by affecting the long-range order pattern of curcumin molecules. Furthermore, there was no additional interaction between the separate components of this complex based on XRD data, which is consistent with earlier research.[23]

3.3.2. Scanning Electron Microscopy. Figure 5A–C show the SEM images of CUR, GO, and the CUR-GO-loaded

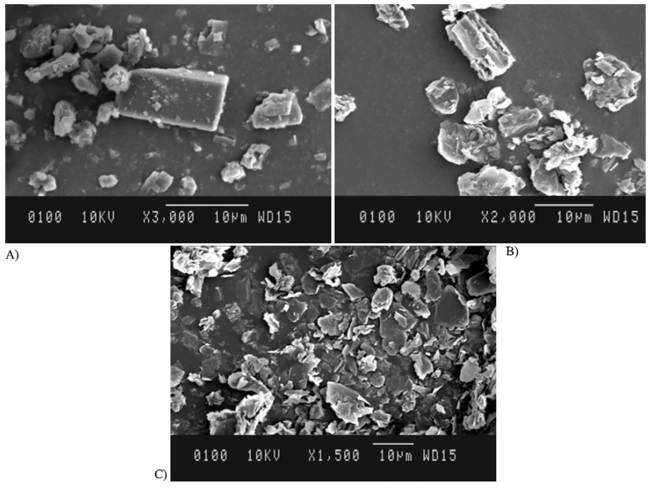

Figure 5. SEM images of (A) CUR, (B) GO, and (C) CUR-GO complex.

complex, respectively. The crystals of pure curcumin were small and consistent in shape, with a surface that seemed to be completely smooth. The GO images show a fluffy appearance, indicating its noncrystalline nature. Because of its fluffy and porous nature with a rough surface, the complex may have formed by undergoing a phase shift without a well-defined geometry. Overall, it concludes that SEM data confirmed the formation of an amorphous phase in the resulting complex, as observed in the PXRD data. Furthermore, the confirmation of the phase shift in the complex is supported with the published literature.[23,30]

3.3.3. Development of Complex-Loaded Liposomes. The detailed methods of preparation of liposomes are described in Section 2.2.5. The thin dry film formed in a RBF hydrated with 10 mL of PBS resulted to form liposomes, which had to be kept overnight and aided with sonication for 5 min to achieve nanosize. For complex development, loaded liposomes as the complex mixture were added in the lipidic phase in the required quantity. Furthermore, the developed liposomes were taken further for the stability study.

3.3.4. Stability Studies of Liposomes. 3.3.4.1. PS, PDI, and Zeta Potential. The developed liposome formulations were stored at 2 to 8 °C, 25 °C/60%RH, and 40 °C/75%RH for 3 months, which resulted to obtain the PS of 184.4 ± 0.41, 184.6 ± 0.25, and 188.34 ± 0.41 nm, respectively. Particle growth was found to be much slower in the case of storage at 2−8 °C and 25 °C/60% RH and concluded that the PS of the stored formulation at the 2−8 °C and 25 °C/60% RH was almost a fairly constant size, or nonsignificant variations were observed (shown in Table 1). At the 40%/75% RH, the stored formulation led to increased collisions among the PS, resulting to form aggregated and enhanced PSs, leading to instability (shown in Table 1).[25] In the other side, the PDI values were 0.269 ± 0.04 and 0.289 ± 0.05, and these values showed physical stability in terms of homogeneity at the temperature of 2−8 °C and 25 °C/60% RH for at least 3 months (shown in Table 1). While in the case of 40%/75% RH, it led to an increased PDI value (0.453 ± 0.06) and led to instability. Zeta potential is the other part of stability determination and not significantly varied over the 3 months of storage at 2−8 °C and 25 °C/60% RH. Moreover, the higher negative zeta potential led to improved stability, which is also supported by the published literature.[24,25] At the 40 °C/75% RH, the zeta potential value showed significant variations in the three-month duration (shown in Table 1). Moreover, this may be due to the increased PS and neutralization of the charges on the surface of liposomes, resulting in heterogeneous dispersion,

https://doi.org/10.1021/acsomega.2c03940
ACS Omega 2022, 7, 43499−43509

Table 1. Stability Data of the Liposomes

formulations	storage condition	time	PS (nm)	PDI	zeta potential
liposome		initial	184 ± 0.31	0.262 ± 0.04	−0.542 ± 0.04
	2−8 °C	1 months	184.1 ± 0.21	0.263 ± 0.05	−0.545 ± 0.05
		2 months	184.3 ± 0.42	0.267 ± 0.02	−0.547 ± 0.03
		3 months	184.4 ± 0.41	0.269 ± 0.04	−0.549 ± 0.04
liposome	25 ± 2 °C/60 ± 5%RH	1 months	184.2 ± 0.35	0.266 ± 0.23	−0.548 ± 0.02
		2 months	184.4 ± 0.22	0. 268 ± 0.04	−0.551 ± 0.03
		3 months	184.6 ± 0.25	0.289 ± 0.05	−0.554 ± 0.01
liposome	40 ± 2 °C/75 ± 5%RH	1 months	184.7 ± 0.24	0.267 ± 0.04	−0.557 ± 0.05
		2 months	186.5 ± 0.52	0.321 ± 0.06	−0.359 ± 0.02
		3 months	188.34 ± 0.41	0.453 ± 0.06	−0.171 ± 0.03

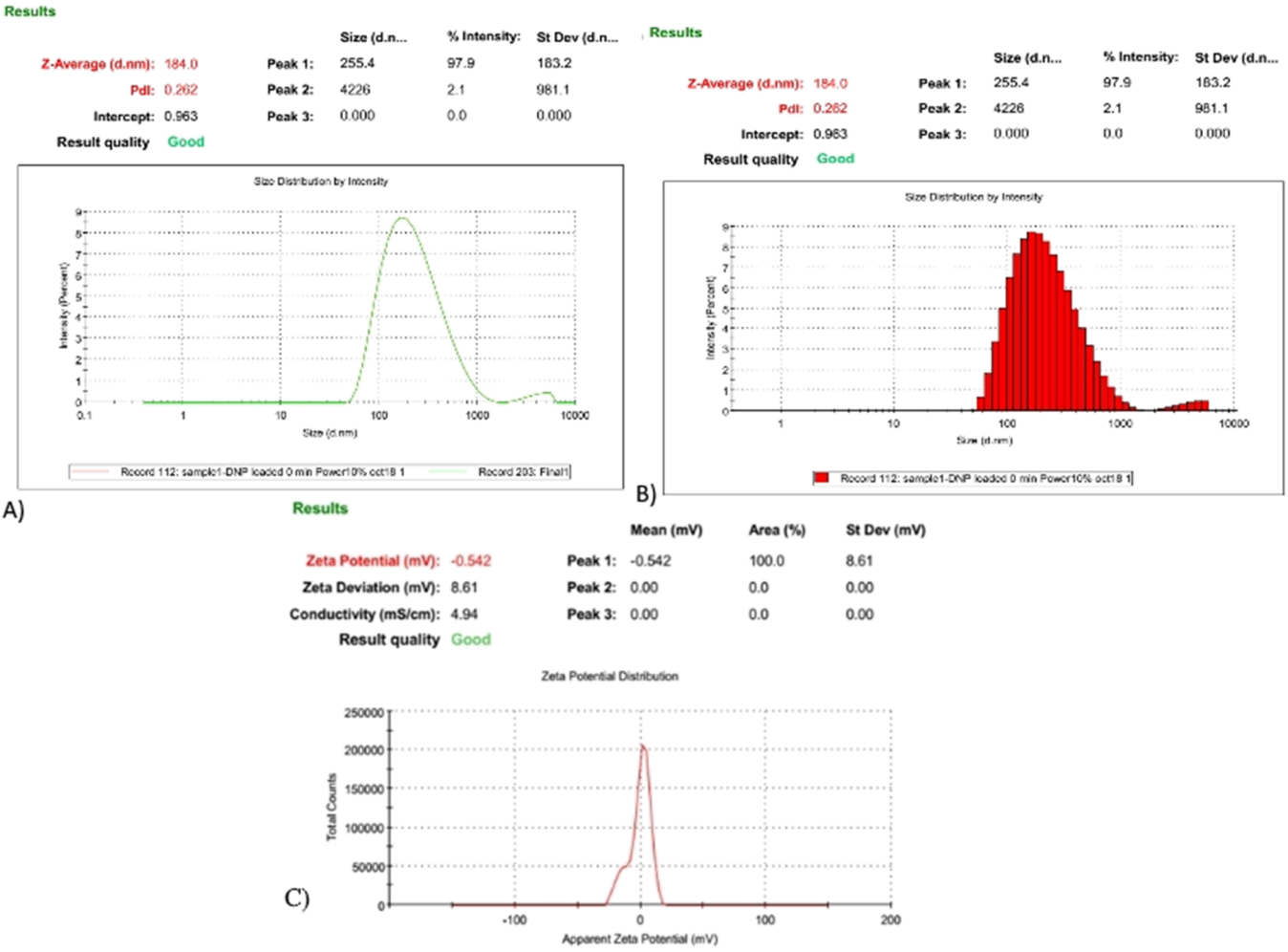

Figure 6. (A, B) Particle size distribution curve of CUR-GO-loaded liposomes and (C) zeta potential of characterized CUR-GO-loaded liposomes.

which is unfavorable.[25] Furthermore, from the above microscopic data, it concludes that the liposomal formulation was stable at 2−8 °C and 25 °C/60% RH and was considered for the next level of study. Additionally, Figure S2 reveals that there are no changes in the physical appearance, and neither there was any growth of microorganisms nor drug-loaded formulation was found clear throughout at the temperatures of 2−8 °C and 25 °C/60% RH; hence, it is stable.

3.3.5. Characterization of Liposome Formulation. 3.3.5.1. PS, Size Distribution, and Zeta Potential. The liposomes showed a PS of 184 ± 0.31 nm, with a PDI of 0.262 ± 0.04 (Figure 6A,B). Furthermore, the zeta potential value was −0.542 ± 0.04 (as shown in Figure 6C). The observed data revealed the nanometric scale of the formulation with homogeneous dispersion of the liposomal formulation. Moreover, the negative value of the zeta potential may be attributed to the presence of fatty acids in lipids and possess anionic surface charge on liposomes, and the lower negative charge may enhance the drug entrapment in vesicle and enhanced cellular uptake in topical drug delivery.[21,26]

3.3.5.2. Photo Microscopy. The optical photomicrographs showed that the liposomes had a consistent vesicular shape, homogeneity, and no aggregation was observed (as shown in Figure 7A). Thus, this finding is supported with the similar findings observed in the published literature.[2]

https://doi.org/10.1021/acsomega.2c03940
ACS Omega 2022, 7, 43499−43509

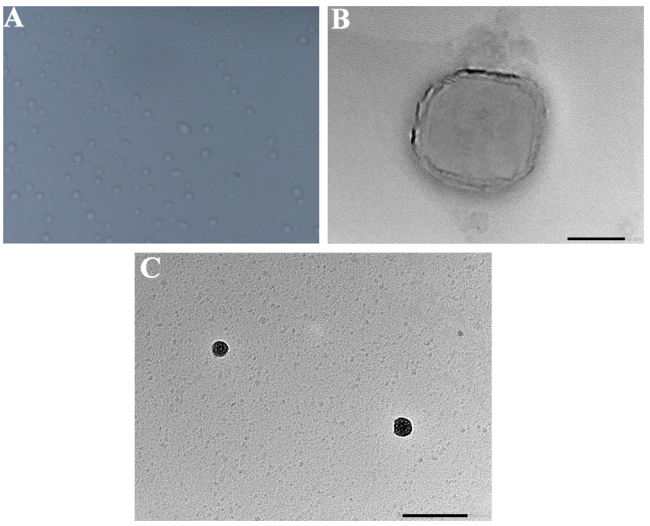

Figure 7. (A) Photo microscopy of stable CUR-GO-loaded liposomes. (B) HR-TEM image of blank-loaded liposome. (C) HR-TEM image of complex-loaded liposomes.

3.3.5.3. High-Resolution Transmission Electron Microscopy. For the liposomes containing CUR + GO, the spherical shape and nanometer size were achieved. The comparative analysis results of HR-TEM images of the blank and complex-loaded liposomes on HR-TEM images are shown in Figure 7B,C. HR-TEM images of the aforementioned drug-loaded formulation showed that the PS is in the range of 175 to 210 nm. Furthermore, this variation was observed in the value of HR-TEM compared with the dynamic light scattering (DLS) technique. This could be attributed to the formulation size determined in the solid state by HR-TEM, but the hydrodynamic diameter of the formulation was calculated using a zetasizer in the fluid state. Furthermore, the HR-TEM images showed a spherical surface of the aforementioned formulation with a uniform PS distribution. In addition to this, HR-TEM images reveal another striking difference from different small, white, and dense spherical bodies, which show the CUR with GO-loaded complex, which are covered by the lipid vesicle. Therefore, the above finding confirmed the loading of the complex into the liposome's vesicles. As a result, our findings are consistent with those of other researchers, as well as those of previous published articles, and our findings validate their findings.[31]

3.3.6. In Vitro Drug Release Studies. As per *the* in vitro study, CUR-loaded liposomes and CUR-GO complex-loaded liposomes demonstrated biphasic delayed and sustained drug-release properties for up to 24 h. Furthermore, the cumulative drug release was calculated during the first 6 h and it was found by 71.24 and 64.24% for CUR-loaded and CUR-GO-loaded liposomes, respectively, (Figure 8). Moreover, the sustained drug release was observed after 10 h up to 24 h. In the first 6 h of the in vitro drug release, as shown in Figure 8, slower drug release from complex-loaded liposomes over the CUR-loaded liposomes was observed, and it may be attributed to the complex formation that may cause slower drug release. Furthermore, it is supported with the published literature.[27,31] The in vitro drug release kinetics on multiple models were investigated, and it was observed that the first-order model (R^2 = 0.9991) was the best fit for CUR-GO-loaded liposomes (shown in Table 2). The drug release model revealed that the drug release exponent occurred because of the non-Fickian

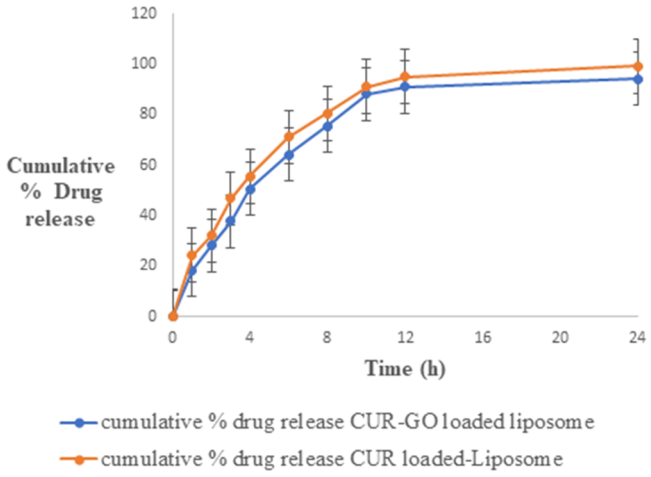

Figure 8. In vitro drug release of CUR-GO-loaded liposome vs CUR-loaded liposome.

Table 2. Drug Release Model (r^2) at Physiological pH of 7.4

formulation	Korsmeyer–Peppas	Higuchi	Hixon–Crowell	first order	
	r^2				n
CUR-GO-loaded liposome	0.952	0.9543	0.9943	0.9991	0.641*
CUR-loaded liposome	0.9892	0.9874	0.9910	0.9973	0.541*

diffusion process, which is often observed to be $n > 0.5$ and is fitted into the first order.[31] Because of their small size and huge surface area, liposomes can release drugs more easily, as observed in CUR liposomes. CUR with GO complex formation led to lower in vitro drug release and more sustained release action over CUR-loaded liposome.[31] Furthermore, the long-lasted sustained drug release action may be exploited for effective topical drug delivery. Additionally, it was concluded that the noncomplex or free drug encapsulated into liposomes caused greater diffusion of drugs across the skin.

3.3.7. Antimicrobial Activity Studies against Staphylococcus aureus. The antibacterial activity of the control, curcumin, GO, the complex (CUR + GO), and complex-loaded liposomes of these components against *Staphylococcus aureus* pathogens could be observed using images of Petri plates taken during the agar well diffusion test. The antibacterial efficacy of the abovementioned formulations was performed and studied. Results from the study showed the efficacy of CUR with GO complex-loaded liposomes which was compared with the efficacy of GO, CUR, and CUR with the GO complex and control also against specific bacteria, as shown in Table 3. Figure 9A,B shows the zone of inhibition obtained from the various test samples. The results obtained confirmed the synergistic antimicrobial activity of CUR with GO-loaded liposomes. The order of bacterial growth inhibition in terms of zones of inhibition was observed as follows:

Control for Petri plate A (13.21 ± 0.32) > Control for Petri plate B (13.1 ± 0.42) > CUR with GO-loaded liposome (D2) Petri plate B (10.7 ± 0.34) > CUR with GO-loaded liposome (D1) for Petri plate B (10.21 ± 0.21) > CUR liposome for Petri plate B (9.21 ± 0.43) > Complex dispersion for Petri plate A (7.8 ± 0.32) > Curcumin suspension for Petri plate A

https://doi.org/10.1021/acsomega.2c03940
ACS Omega 2022, 7, 43499−43509

Table 3. Zone of Inhibition of Test Samples (n = 3 ± S.D)

test samples	zone of inhibition (mm)
control for Petri plate A	13.21 ± 0.32
control for Petri plate B	13.1 ± 0.42
GO dispersion for Petri plate A	6.15 ± 0.31
curcumin suspension for Petri plate A	7.1 ± 0.21
complex dispersion for Petri plate A	7.8 ± 0.32
CUR liposome for Petri plate B	9.21 ± 0.43
CUR with GO-loaded liposome (D1) for Petri plate B	10.21 ± 0.21
CUR with GO-loaded liposome (D2) Petri plate B	10.7 ± 0.34

A) B)

Figure 9. (A, B) Zone of inhibition of various formulation and control formulation at various doses (Dose 1 and Dose 2) against *S. aureus*.

(7.1 ± 0.21) > GO dispersion for Petri plate A (6.15 ± 0.31). As all components were dissolved in ethanol, it was run as a control to nullify its effects in every well. Moreover, the CUR with GO-loaded liposome (D2) Petri plate B is 10.7 ± 0.34 which offered higher anti-microbial activity over other formulations (shown in Table 3) against the mentioned bacterial microorganism that causes skin diseases. Therefore, this experimental data conclude the highest antimicrobial action of complex-loaded liposomes of D2 in Petri plate B, which may be due to the synergistic effects produced by the complex-loaded liposomes over pure CUR-loaded liposomes.

4. DISCUSSION

Curcumin has low water solubility, making it difficult for curcumin to be topically permeated.[9,32] Despite its diverse pharmacological effects, commercially available medications fall short of expectations. GO has exceptional water dispersibility, amphiphilicity, surface functionality, and large specific surface area that have made it a major focus in drug delivery research. For its biocompatibility and low cytotoxicity, this new material has been intensively explored for drug delivery, such as treatment against bacterial infections.[7,8] Researchers have shown that GO colloidal suspensions and other graphene-oxide-based nanomaterials are effective drug carriers. It is possible to attach drug molecules via van der Waal's forces, covalent bonding, or noncovalent stacking.[8] To increase the solubility of curcumin, it was conjugated with GO. For decades, liposomes have played an essential role in drug delivery. When compared to competing conventional products, it may perform better in drug delivery and therapeutics. Using liposomes in topical drug delivery systems has become more popular because of their amphiphilic character, which makes them an excellent penetration enhancer for the cutaneous drug delivery of various phytoactives including curcumin.[33] According to the literature, the loading of various phytoactives with GO has been available for various therapeutics.[7,13−15] In our experiment, CUR with the GO complex has been developed, and further, it is loaded into the liposomes. The complex formation resulted in a ratio of 1:1 (CUR: GO), as shown in Figure S1. Furthermore, the complex formation confirmation was observed from the UV spectra (Figure 3b), which showed shifting in the peak of the complex over pure CUR. After this, for liposomal development, solubility measurement is an important consideration, and results show that CUR exhibits the highest solubility in DMSO as the solvent and in in vitro release media PBS with ethanol 80: 20 v/v. After that, the CUR solubility in various lipids was observed in tripalmitin. On the other hand, the solubility of GO was the highest in DMSO and the highest solubility of lipid was found in tripalmitin. Therefore, both selected excipients are to play an important role in the development of liposomes. The higher solubility of the drug in lipids and solvent is an important consideration in topical permeation and drug deposition into the skin.[15,16,31] The XRD pattern of CUR showed that it has a halo pattern with few diffraction peaks, thus indicating a partial amorphous nature of the sample (Figure 4B) while GO showed an amorphous pattern with a broad 2θ peak at 11.2 (Figure 4C). Besides, the PXRD results of the complex (CUR with GO) showed a broad halo pattern, confirming the amorphous nature of the resulting complex (Figure 4D). Therefore, the summary of the above results showed that the presence of GO facilitates the amorphization of the resulting complex by affecting the long-range order pattern of curcumin molecules. Another study in characterization is SEM images, which reflected the amorphous phase in the formed complex, as observed in the PXRD data over the pure CUR. Therefore, it is summarized that shifting in the complex phase is supported by the published literature also.[23] Finally, the liposomes were developed using a rota-evaporator and taken for a stability study. The stability study results during 3 months at 2−8 °C and 25 °C/60% RH are shown in Table 1; the microscopic data in terms of the PS, PDI, and zeta potential remined nonsignificantly varied and at stressed conditions (40 ± 2 °C/75 ± 5%RH), and it revealed significant variations in the aforementioned parameter. Additionally, from Figure S2, it can be seen that there are no changes in the physical appearance and throughout the 3-month duration, and it seems clear with no sedimentation observed. Furthermore, the characterization of stable liposomes revealed 184 ± 0.31 nm, with a PDI of 0.262 ± 0.04 and a zeta potential value of −0.542 ± 0.04. Therefore, the above results are summarized in the nanometric scale of the formulation with homogeneity. Moreover, the zeta potential values come under the range for stability, as supported by the published literature. The photo microscopy image revealed a consistent vesicular shape and homogeneity, and no aggregation was observed. The HR-TEM image revealed a size in the range of 175 to 210 nm, which is little varied from the DLS data. This variation is attributed to the particle size determined in the solid state by HR-TEM. In DLS, the hydrodynamic diameter of the formulation was measured using a zeta sizer in the fluid state. In addition to this, HR-TEM images reveal another striking difference from different small, white, and dense spherical bodies, which show encapsulated CUR with the GO-loaded complex, which are covered by the lipid vesicle as from the in vitro drug release study; CUR-loaded liposomes and the complex-loaded liposomes show sustained drug release up to the end of 24 h. Moreover, the cumulative drug release in the initial 6 h was observed to be

https://doi.org/10.1021/acsomega.2c03940
ACS Omega 2022, 7, 43499−43509

64.24% with complex-loaded liposomes over CUR liposomes (71.24%). The slower drug release is attributed to the complexation of CUR with GO. Moreover, the long-lasting sustained drug release action with the complex-loaded liposomes may be exploited for the effective topical drug delivery. In the last, the antimicrobial study observed the highest antimicrobial action with complex-loaded liposomes in D2 of Petri plate B, as shown in Table 3. After this, CUR-loaded liposomes were observed the second highest antimicrobial action. The first highest antimicrobial action is attributed to the synergistic effects produced by the combined use of CUR with GO.

5. CONCLUSIONS

This work was to develop complex (CUR + GO complex), and its characterization was investigated. After that, it is loaded into liposomes. In the complex development, its identification is confirmed through UV spectra, whereas showing shifting in the peak confirmed the complex formation. In the preformulating work, the highest drug and GO solubility were observed in DMSO and tripalmitin. Both selected excipients are important in the liposome's development. The complex is characterized by XRD, and it results in amorphization by affecting the long-range order pattern of CUR. Furthermore, there was no additional interaction between the separate components of this complex based on the XRD data. The SEM data confirmed the formation of an amorphous phase in the resulting complex, as observed in the PXRD data. Furthermore, the liposomes were formed using the film evaporator method and stability data for 3 months, concluding that they were stable at 2−8 °C and 25 °C/60% RH. Additionally, there is no physical separation or sedimentation observed. The DLS and optical microscopy data were found on the nanometric scale of PS with the homogeneity of liposomes without any aggregation. CUR with GO complex formation led to lower in vitro drug release and more sustained release action over CUR-loaded liposomes. Furthermore, the long-lasted sustained drug release action may be exploited for effective topical drug delivery. Whereas the antimicrobial data reported the highest antimicrobial action of complex-loaded liposomes of D2 in Petri plate B, this may be due to the synergistic effects produced by the complex-loaded liposomes over pure CUR-loaded liposomes. Therefore, the in vivo studies on animals must establish in vivo results with biocompatible studies in the future.

■ ASSOCIATED CONTENT

Supporting Information

The Supporting Information is available free of charge at https://pubs.acs.org/doi/10.1021/acsomega.2c03940.

(Figure S1) curcumin with GO complex formation at the ratio of 1:1; (Figure S2A,B) stability images showing no changes in physical appearance and other evaluation parameters at (A) 2−8 °C and (B) 25 ± 2 °C/60 ± 5% RH (PDF)

■ AUTHOR INFORMATION

Corresponding Author

Mahfoozur Rahman − *Department of Pharmaceutical Sciences, Shalom Institute of Health & Allied Sciences, Sam Higginbottom University of Agriculture, Technology & Sciences, Allahabad 211007, India;* orcid.org/0000-0002-5616-4026; Email: mahfoozkaifi@gmail.com

Authors

Joina Gunjan Singh − *Department of Pharmaceutical Sciences, Shalom Institute of Health & Allied Sciences, Sam Higginbottom University of Agriculture, Technology & Sciences, Allahabad 211007, India*

Obaid Afzal − *Department of Pharmaceutical Chemistry, College of Pharmacy, Prince Sattam Bin Abdulaziz University, Alkharj 11942, Saudi Arabia*

Abdulmalik Saleh Alfawaz Altamimi − *Department of Pharmaceutical Chemistry, College of Pharmacy, Prince Sattam Bin Abdulaziz University, Alkharj 11942, Saudi Arabia*

Majed Alrobaian − *Department of Pharmaceutics and Industrial Pharmacy, College of Pharmacy, Taif University, Taif 21944, Saudi Arabia*

Jamshed Haneef − *Department of Pharmaceutical Chemistry, School of Pharmaceutical Education and Research, New Delhi 110062, India*

Md. Abul Barkat − *Department of Pharmaceutics, College of Pharmacy, University of Hafr Al Batin, Hafr Al Batin 39524, Saudi Arabia;* orcid.org/0000-0001-6009-5222

Waleed H Almalki − *Department of Pharmacology and Toxicology, College of Pharmacy, Umm Al-Qura University, Makkah 24382, Saudi Arabia*

Mayank Handa − *Department of Pharmaceutics, National Institute of Pharmaceutical Education and Research-Raebareli, Lucknow, UP 226002, India;* orcid.org/0000-0001-9093-6432

Rahul Shukla − *Department of Pharmaceutics, National Institute of Pharmaceutical Education and Research-Raebareli, Lucknow, UP 226002, India;* orcid.org/0000-0002-4864-0133

Shehla Nasar Mir Najib Ullah − *Department of Pharmacognosy, Faculty of Pharmacy, King Khalid University, Abha 62529, Saudi Arabia*

Vikas Kumar − *Department of Pharmaceutical Sciences, Shalom Institute of Health & Allied Sciences, Sam Higginbottom University of Agriculture, Technology & Sciences, Allahabad 211007, India;* orcid.org/0000-0001-9984-0437

Sarwar Beg − *Department of Pharmaceutics, School of Pharmaceutical Education and Research, Jamia Hamdard, New Delhi 110062, India;* orcid.org/0000-0002-3304-2712

Complete contact information is available at: https://pubs.acs.org/10.1021/acsomega.2c03940

Notes

The authors declare no competing financial interest.

The authors confirm that the data supporting the findings of this study are available within the articles and can be shared upon request.

■ ACKNOWLEDGMENTS

The authors extend their appreciation to the Deputyship for Research and Innovation, Ministry of Education in Saudi Arabia, for funding this research work through project number 20-UQU-IF-P1-001. The authors would like to thank the Deanship of Scientific Research at Umm Al-Qura University for supporting this work by Grant code (22UQU4310387DSR36). The authors also extend their appreciation to the Deanship of Scientific Research at King

https://doi.org/10.1021/acsomega.2c03940
ACS Omega 2022, 7, 43499−43509

Khalid University for funding this work through small group project under grant number RGP.1/173/43.

REFERENCES

(1) Clebak, K. T.; Malone, M. A. Skin Infections. *Prim. Care.* **2018**, *45*, 433−454.
(2) Chen, L.; Alrobaian, M.; Afzal, O.; Kazmi, I.; Panda, S. K.; Altamimi, A. S. A.; Rahman, M.; et al. Crotamiton-loaded tea tree oil containing phospholipid-based microemulsion hydrogel for scabies treatment: *in vitro*, *in vivo* evaluation, and dermatokinetic studies. *Drug Deliv.* **2021**, *28*, 1972−1981.
(3) Rahman, M.; Beg, S. Perspective in Topical Infective and Non-infective Skin Diseases Therapy with Emergence of Nanomedicine. *Recent Pat. Antiinfect. Drug Discov.* **2019**, *14*, 3−4.
(4) Hussain, Y.; Alam, W.; Ullah, H.; Dacrema, M.; Daglia, M.; Khan, H.; Arciola, C. R. Antimicrobial Potential of Curcumin: Therapeutic Potential and Challenges to Clinical Applications. *Antibiotics (Basel)* **2022**, *11*, 322.
(5) Almarzoky-Abuhussain, S. S.; Goodlet, K. J.; Nailor, M. D.; Nicolau, D. P. Optimizing skin and skin structure infection outcomes: considerations of cost of care. *Expert Rev. Pharmacoecon. Outcomes Res.* **2018**, *18*, 235−244.
(6) Rahman, M.; Akhter, S.; Ahmad, M. Z.; Ahmad, J.; Addo, R. T.; Ahmad, F. J.; Pichon, C. Emerging advances in cancer nano-theranostics with graphene nanocomposites: opportunities and challenges. *Nanomedicine (Lond)* **2015**, *10*, 2405−2422.
(7) Khalil, W. F.; El-Sayyad, G. S.; El Rouby, W. M. A.; Sadek, M. A.; Farghali, A. A.; El-Batal, A. I. Graphene oxide-based nanocomposites (GO-chitosan and GO-EDTA) for outstanding antimicrobial potential against some Candida species and pathogenic bacteria. *Int. J. Biol. Macromol.* **2020**, *164*, 1370−1383.
(8) Esquivel, G. C.; Cervantes-Cuevas, H.; Ybieta-Olvera, L. F.; Castañeda Briones, M. T.; Acosta, D.; Cabello, J. Antimicrobial activity of graphite oxide doped with silver against *Bacillus subtilis*, *Candida albicans*, *Escherichia coli*, and *Staphylococcus aureus* by agar well diffusion test: Synthesis and characterization. *Mater. Sci. Eng., C Mater. Biol. Appl.* **2021**, *123*, No. 111934.
(9) Chen, Y.; Lu, Y.; Lee, R. J.; Xiang, G. Nano Encapsulated Curcumin: And Its Potential for Biomedical Applications. *Int. J. Nanomedicine* **2020**, *15*, 3099−3120.
(10) Rapalli, V. K.; Kaul, V.; Gorantla, S.; Waghule, T.; Dubey, S. K.; Pandey, M. M.; Singhvi, G. UV Spectrophotometric method for characterization of curcumin loaded nanostructured lipid nanocarriers in simulated conditions: Method development, in-vitro and ex-vivo applications in topical delivery. *Spectrochim. Acta A Mol. Biomol. Spectrosc.* **2020**, *224*, No. 117392.
(11) Rajasekar, V.; Darne, P.; Prabhune, A.; Kao, R. Y. T.; Solomon, A. P.; Ramage, G.; Samaranayake, L.; Neelakantan, P. A curcumin-sophorolipid nanocomplex inhibits Candida albicans filamentation and biofilm development. *Colloids Surf., B Biointerfaces* **2021**, *200*, No. 111617.
(12) De, D.; Das, C. K.; Mandal, D.; Mandal, M.; Pawar, N.; Chandra, A.; Gupta, A. N. Curcumin Complexed with Graphene Derivative for Breast Cancer Therapy. *ACS Appl. Bio Mater.* **2020**, *3*, 6284−6296.
(13) Cobos, M.; De-La-Pinta, I.; Quindós, G.; Fernández, M. J.; Fernández, M. D. Graphene Oxide-Silver Nanoparticle Nanohybrids: Synthesis, Characterization, and Antimicrobial Properties. *Nanomaterials (Basel)* **2020**, *10*, 376.
(14) Hussein-Al-Ali, S. H.; Abudoleh, S. M.; Hussein, M. Z.; Bullo, S.; Palanisamy, A. Graphene oxide-ellagic acid nanocomposite as effective anticancer and antimicrobial agent. *IET Nanobiotechnol.* **2021**, *15*, 79−89.
(15) Su, Z.; Sun, D.; Zhang, L.; He, M.; Jiang, Y.; Millar, B.; Douglas, P.; Mariotti, D.; Maguire, P.; Sun, D. Chitosan/Silver Nanoparticle/Graphene Oxide Nanocomposites with Multi-Drug Release, Antimicrobial, and Photothermal Conversion Functions. *Materials (Basel)* **2021**, *14*, 2351.
(16) Alavi, M.; Adulrahman, N. A.; Haleem, A. A.; Al-Râwanduzi, A. D. H.; Khusro, A.; Abdelgawad, M. A.; Ghoneim, M. M.; Batiha, G. E.; Kahrizi, D.; Martinez, F.; Koirala, N. Nanoformulations of curcumin and quercetin with silver nanoparticles for inactivation of bacteria. *Cell Mol. Biol. (Noisy-le-grand)* **2022**, *67*, 151−156.
(17) Liu, G.; Hou, S.; Tong, P.; Li, J. Liposomes: Preparation, Characteristics, and Application Strategies in Analytical Chemistry. *Crit. Rev. Anal. Chem.* **2022**, *52*, 392−412.
(18) Wahyudiono; He, J.; Hu, X.; Machmudah, S.; Yasuda, K.; Takami, S.; Kanda, H.; Goto, M. Curcumin-Loaded Liposome Preparation in Ultrasound Environment under Pressurized Carbon Dioxide. *Foods* **2022**, *11*, 1469.
(19) Ansari, M. J.; Rahman, M.; Alharbi, K. S.; Altowayan, W. M.; Ali, A. M. A.; Almalki, W. H.; Barkat, M. A.; Singh, T.; Nasar, S.; Akhter, M. H.; Beg, S.; Choudhry, H. Hispolon-Loaded Liquid Crystalline Nanoparticles: Development, Stability, In Vitro Delivery Profile, and Assessment of Hepatoprotective Activity in Hepatocellular Carcinoma. *ACS Omega* **2022**, *7*, 9452−9464.
(20) Fathima, T. K. S.; Banu, A. A.; Devasena, T.; Ramaprabhu, S. A novel, highly sensitive electrochemical 1,4-dioxane sensor based on reduced graphene oxide curcumin nanocomposite. *RSC Adv.* **2022**, *12*, 19375−19383.
(21) Maqbool, F.; Moyle, P. M.; Tan, M. S. A.; Thurecht, K. J.; Falconer, J. R. Preparation of albendazole-loaded liposomes by supercritical carbon dioxide processing. *Artif. Cells Nanomed. Biotechnol.* **2018**, *46*, S1186−S1192.
(22) Chatterjee, P.; Dutta, S. S.; Chakraborty, T. Tautomers and Rotamers of Curcumin: A Combined UV Spectroscopy, High-Performance Liquid Chromatography, Ion Mobility Mass Spectrometry, and Electronic Structure Theory Study. *J. Phys. Chem. A.* **2022**, *126*, 1591−1604.
(23) Rathi, P.; Singh, D. P.; Surain, P. Synthesis, characterization, powder XRD and antimicrobial-antioxidant activity evaluation of trivalent transition metal macrocyclic complexes. *C. R. Chim.* **2015**, *18*, 430−437.
(24) Zhang, Y.; Jing, Q.; Hu, H.; He, Z.; Wu, T.; Guo, T.; Feng, N. Sodium dodecyl sulfate improved stability and transdermal delivery of salidroside-encapsulated niosomes via effects on zeta potential. *Int. J. Pharm.* **2020**, *580*, No. 119183.
(25) Tai, K.; Rappolt, M.; Mao, L.; Gao, Y.; Yuan, F. Stability and release performance of curcumin-loaded liposomes with varying content of hydrogenated phospholipids. *Food Chem.* **2020**, *326*, No. 126973.
(26) Miranda-Cadena, K.; Dias, M.; Costa-Barbosa, A.; Collins, T.; Marcos-Arias, C.; Eraso, E.; Pais, C.; Quindós, G.; Sampaio, P. Erratum for Miranda-Cadena et al., Development and Characterization of Monoolein-Based Liposomes of Carvacrol, Cinnamaldehyde, Citral, or Thymol with Anti-Candida Activities. *Antimicrob. Agents Chemother.* **2021**, *65*, e00800−e00821.
(27) Zafar, A.; Imam, S. S.; Alruwaili, N. K.; Yasir, M.; Alsaidan, O. A.; Alshehri, S.; Ghoneim, M. M.; Khalid, M.; Alquraini, A.; Alharthi, S. S. Formulation and Evaluation of Topical Nano-Lipid-Based Delivery of Butenafine: In vitro Characterization and Antifungal Activity. *Gels* **2022**, *8*, 133.
(28) Ontong, J. C.; Singh, S.; Nwabor, O. F.; Chusri, S.; Voravuthikunchai, S. P. Potential of antimicrobial topical gel with synthesized biogenic silver nanoparticle using Rhodomyrtus tomentosa leaf extract and silk sericin. *Biotechnol. Lett.* **2020**, *42*, 2653−2664.
(29) Puglisi, A.; Giovannini, T.; Antonov, L.; Cappelli, C. Interplay between conformational and solvent effects in UV-visible absorption spectra: curcumin tautomers as a case study. *Phys. Chem. Chem. Phys.* **2019**, *21*, 15504−15514.
(30) Elkholy, N. S.; Shafaa, M. W.; Mohammed, H. S. Biophysical characterization of lutein or beta carotene-loaded cationic liposomes. *RSC Adv.* **2020**, *10*, 32409−32422.
(31) Madan, S.; Nehate, C.; Barman, T. K.; Rathore, A. S.; Koul, V. Design, preparation, and evaluation of liposomal gel formulations for

https://doi.org/10.1021/acsomega.2c03940
ACS Omega 2022, 7, 43499−43509

treatment of acne: in vitro and in vivo studies. *Drug Dev. Ind. Pharm.* **2019**, *45*, 395−404.
(32) Ipar, V. S.; Dsouza, A.; Devarajan, P. V. Enhancing Curcumin Oral Bioavailability Through Nanoformulations. *Eur. J. Drug Metab. Pharmacokinet.* **2019**, *44*, 459−480.
(33) Wang, Y.; Ding, R.; Zhang, Z.; Zhong, C.; Wang, J.; Wang, M. Curcumin-loaded liposomes with the hepatic and lysosomal dual-targeted effects for therapy of hepatocellular carcinoma. *Int. J. Pharm.* **2021**, *602*, No. 120628.

https://doi.org/10.1021/acsomega.2c03940
ACS Omega 2022, 7, 43499−43509